Journal of Southeast University (English Edition) Vol. 31, No. 1, pp. 124 - 129 Mar. 2015 ISSN 1003—7985

Experimental validation of horizontal joints in an innovative totally precast shear wall system

Sun Jian[1] Qiu Hongxing[1] Lu Bo[2]

([1]Key Laboratory of Concrete and Prestressed Concrete Structures of Ministry of Education, Southeast University, Nanjing 210096, China)

([2]Suzhou Institute of Architectural Design Co., Ltd., Suzhou 215021, China)

Abstract: To investigate the feasibility and seismic performance of the horizontal joints in an innovative precast shear wall system, two test walls were fabricated, and the monotonic and cyclic loading tests were performed on the two test walls, respectively. Then, the lateral load-top displacement curves, load bearing capacity, ductility, lateral stiffness, strains of steel bars, strain distribution on the connecting steel frame (CSF), and relative slippages between the CSF and embedded limbic steel frame (ELSF) were discussed in detail. The test results show that the load bearing capacity and ductility of the test wall are both favorable with a displacement ductility factor of more than 3.7. The normal and shear stresses in the CSF except for the compression end are far smaller than the yield stresses throughout the test procedure. Certain slippages of about 1.13 mm occurs between the CSF and ELSF on the compression side of the test wall, while almost no slippages occurs on the tension side. The seismic performance of the test wall is favorable and the new-type scheme of the horizontal joints is both feasible and reliable.

Key words: precast shear wall; horizontal joints; seismic performance; feasibility

doi: 10.3969/j.issn.1003-7985.2015.01.021

Precast concrete structures possess many advantages when compared with cast-in-situ concrete structures, such as better construction quality, faster construction speed, fewer shrinkage cracks, etc. In recent years, many researchers around the world have been conducting extensive research on various precast reinforced concrete (RC) shear wall systems. Pavese and Bournas[1] experimentally investigated the behavior of prefabricated RC sandwich panels under simulated seismic loading through a large experimental campaign. Bora et al.[2] proposed a load-limiting connector which allowed precast, prestressed concrete wall panels to act as shear walls without relying on wall ductility or causing an anchorage failure in a thin concrete section of the wall panel. A series of experimental and analytical studies[3-7] were carried out on unbonded post-tensioned walls. Zhu and Guo[8] performed low-cyclic reversed loading tests on new precast concrete shear wall structures. Jiang et al.[9] established a calculation model for the superimposed slab shear walls. However, most of these structures require a certain amount of in-place wet work.

In Ref. [10], we devised an innovative precast shear wall (IPSW) system characterized by no wet work. The horizontal joints in this system utilize an embedded limbic steel frame (ELSF), high strength bolt (HSB), and connecting steel frame (CSF) to join the adjoining upper and lower precast RC wall panels (UWP and LWP) together.

1 Experimental Program

1.1 Specimen details

Two test specimens, denoted as WH-1 and WH-2, were designed and fabricated with the same parameters, including geometries, concrete compression strength, reinforcement ratio, connectors, etc. Fig. 1 schematically shows the details of the test walls. The vertical and horizontal distributing steel bars in the UWP are set to be ϕ6.5 mm@120 mm and ϕ8 mm@120 mm, respectively. The longitudinal steel bars and confined stirrups in the embedded columns are set to be 4ϕ8 mm and ϕ6.5 mm @60 mm, respectively. The symbol ϕ represents Grade HPB235. The steel plates contained in the CSF and ELSF are 10 mm in thickness with Grade Q235. The HSBs are M16 of Grade 10.9 s.

The cube compressive strength of the concrete was 38.9 MPa. The mechanical properties of the steel bars and steel plate are listed in Tab. 1.

1.2 Test setup

WH-1 and WH-2 were both first loaded by a constant axial force of 505 kN and subsequently tested under the monotonic load and the low-cyclic reversed load, respectively. Fig. 2 shows the photograph of the test setup. The axial pressure was exerted by two jacks fixed on the top beam of the test wall, and the lateral load was applied by a horizontally positioned MTS actuator mounted on the reaction wall.

1.3 Measurement scheme

Fig. 3 schematically shows the measurement scheme:

Received 2014-07-01.

Biographies: Sun Jian (1984—), male, graduate; Qiu Hongxing (corresponding author), male, doctor, professor, qiuhx@seu.edu.cn.

Citation: Sun Jian, Qiu Hongxing, Lu Bo. Experimental validation of horizontal joints in an innovative totally precast shear wall system[J]. Journal of Southeast University (English Edition), 2015, 31(1): 124 - 129. [doi: 10.3969/j.issn.1003-7985.2015.01.021]

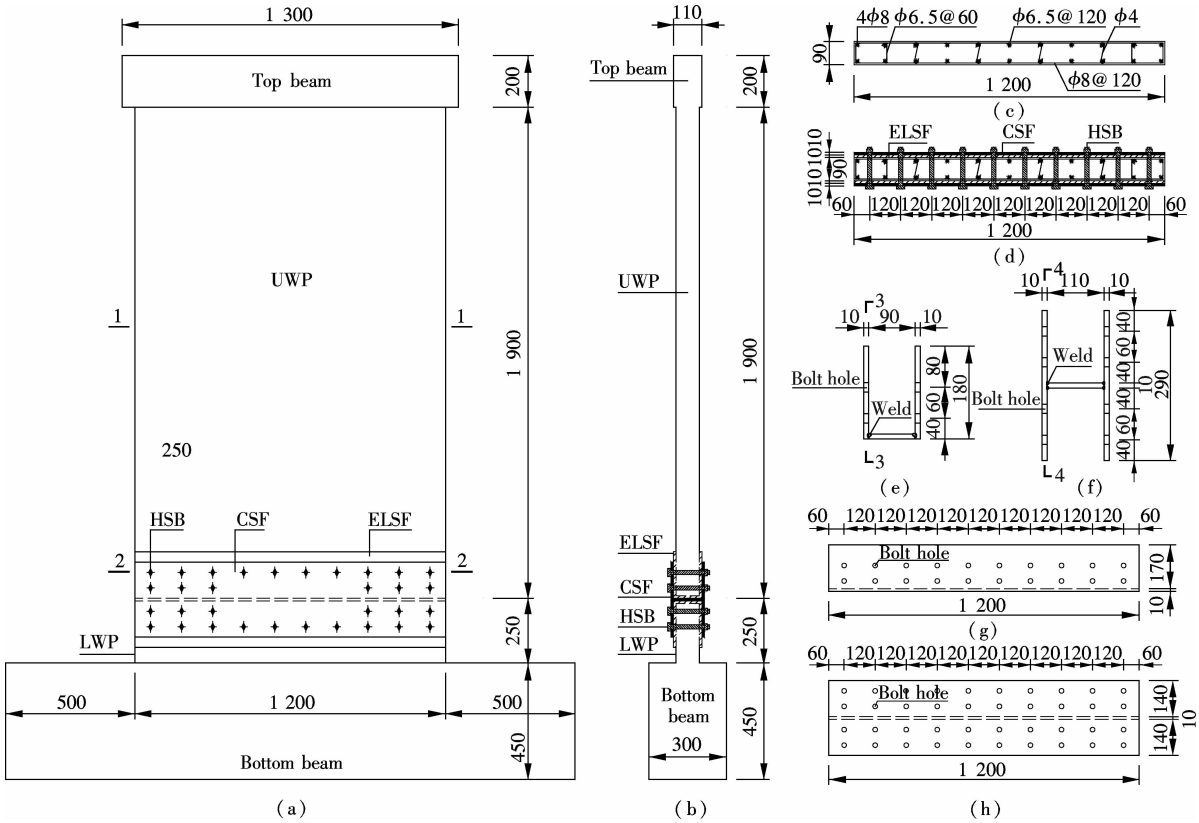

Fig. 1 Fabrication details. (a) Front view; (b) Lateral view; (c) 1-1; (d) 2-2; (e) ELSF; (f) CSF; (g) 3-3; (h) 4-4 (unit: mm)

Tab. 1 Material properties

Material	Yield strength f_y/MPa	Tensile strength f_u/MPa	Modulus of elasticity E_s/GPa
ϕ8	303	461	210
ϕ6.5	382	525	210
Steel plate	259	385	206

Fig. 2 Test setup

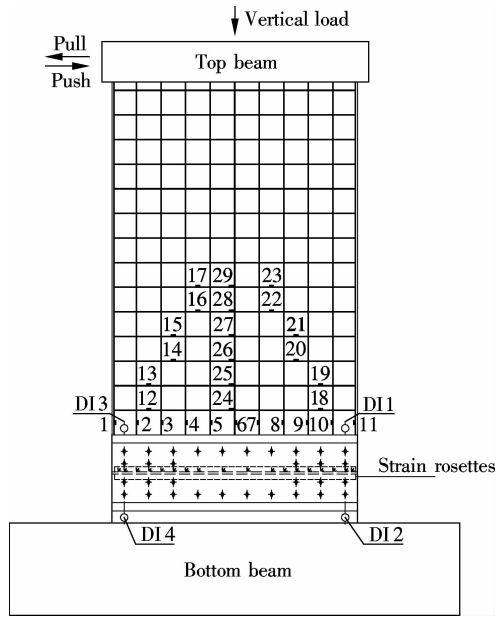

Fig. 3 Measurement scheme

1) A displacement meter and load transducer were fixed on the MTS actuator to measure the horizontal displacement and force; 2) Four dial indicators (DI1 to DI4) were fixed on the CSF and ELSF to measure the relative slippages between them; 3) A number of strain rosettes were bonded on the CSF to measure the strain distribution; and 4) The strains of the vertical steel bars and horizontal steel bars were measured by Nos. 1-11 and Nos. 12-29 strain gauges, respectively.

2 Test Phenomena

2.1 WH-1

The first crack formed at the tension corner when the lateral force reached 100 kN. Afterwards, when the lateral force reached 160 kN, the load-displacement curve became bent and the outmost vertical steel bar yielded on the tension side. After that, the loading procedure was

converted to displacement-controlled mode. In the course of the top displacement increasing from the yield displacement Δ_y to 24.7 mm, some new horizontal cracks formed on the tension side and then evolved into diagonal cracks; meanwhile the vertical steel bars sequentially reached their yield strain from the outmost to the 7th on the tension side. When the top displacement reached 43.6 mm, the diagonal cracks extended to the compressive zone and the concrete at the tension corner began to spall. When the top displacement reached 68.6 mm, the first crack increased to 10 mm in width and extended to the edge of the compressive zone; and the concrete at the compression corner began to spall. Eventually, when the top displacement reached 74.6 mm, the concrete at the compression corner spalled and was crushed in a large area accompanied by the exposure of the horizontal steel bars and the buckling of the vertical steel bars; meanwhile the lateral load decreased by an amount greater than 15%. Fig. 4 shows the failure mode of WH-1.

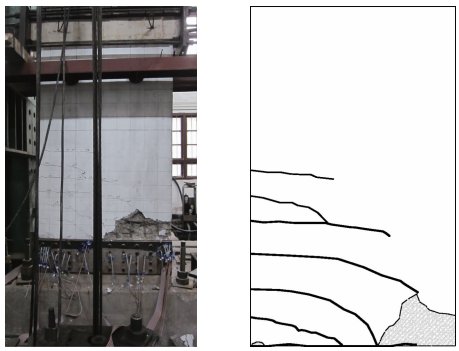

Fig. 4 Failure mode of WH-1. (a) Photograph; (b) Crack pattern

2.2 WH-2

When the pull load reached 120 kN, the first crack formed at the tension corner. However, in the push direction, the first crack at the tension corner occurred when the push load increased to 100 kN. Afterwards, a number of newly-developed cracks occurred and meanwhile the existing cracks constantly expanded and extended. When the lateral force reached 160 kN, the outmost vertical steel bar yielded on the tension side. After that, the loading procedure was changed to the displacement-controlled mode. With the increase in the top displacement, the existing diagonal cracks became crossed. Eventually, during the first cycle of $5\Delta_y$ in the pull direction, the concrete at the compression corner crushed and spalled in a large area resulting in more than 15% decrease of the lateral force. Fig. 5 shows the failure mode of WH-2.

3 Experimental Results and Discussion

3.1 Load-displacement curves

Fig. 6 shows the load-displacement curves of the two

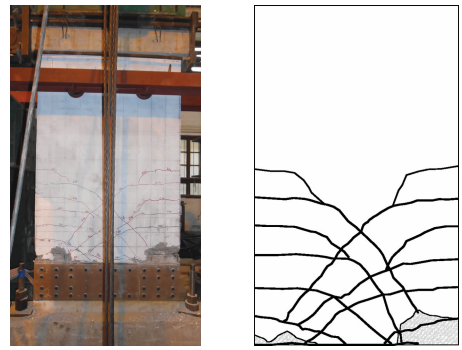

Fig. 5 Failure mode of WH-2. (a) Photograph; (b) Crack pattern

test specimens. It can be known from Fig. 6 that: 1) Although the design and fabrication of the two test walls are identical, the ultimate displacement of WH-1 is much greater than that of WH-2; and 2) As for WH-2, during the first cycle of $4\Delta_y$, the lateral force reaches the maximum values of 294.24 and 270.10 kN with the corresponding top displacements of 43.79 and 43.49 mm in push and pull directions, respectively.

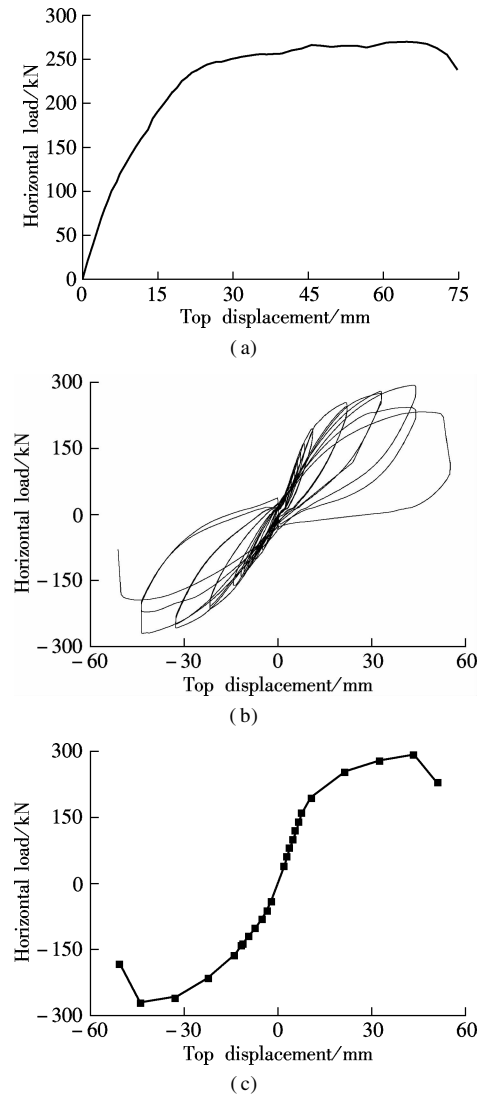

Fig. 6 Load-displacement curves. (a) Load-displacement curve of WH-1; (b) Hysteretic loop of WH-2; (c) Skeleton curve of WH-2

3.2 Feature points on the *P*-Δ curves

The test data are listed in Tab. 2. It can be known from this table that: 1) The cracking inter-storey drift angle (Δ_{cr}/H), yield inter-storey drift angle (Δ_y/H), and ultimate inter-storey drift angle (Δ_u/H) of the two test walls are greater than the limiting values in Chinese code[11], and are close to the corresponding values in Refs. [12 − 13], indicating that the deformability of the test wall is relatively good and the lateral stiffness is comparable to the precast shear wall in Refs. [12 − 13]; and 2) The displacement ductility factor shows that the ductility of the test walls is favorable, which reaches more than 3.7.

Tab. 2 Key test data

Test walls	Loading direction	Cracking point			Yield point			Peak point			Ultimate point			Ductility
		F_{cr}/kN	Δ_{cr}/mm	Δ_{cr}/H	F_y/kN	Δ_y/mm	Δ_y/H	F_m/kN	Δ_m/mm	Δ_m/H	F_u/kN	Δ_u/mm	Δ_u/H	μ
WH-1	Push	100	5.76	1/391	160	11.70	1/192	270.13	64.64	1/35	238.88	74.63	1/30	6.4
WH-2	Push	120	5.88	1/383	160	7.92	1/284	294.24	43.79	1/51	230.76	51.39	1/44	6.5
	Pull	100	7.07	1/318	160	13.83	1/163	270.10	43.49	1/51	181.70	50.65	1/44	3.7

3.3 Lateral stiffness

With the ever-increasing top displacement, the lateral stiffness gradually decreased due to the accumulated damage in the test wall. To evaluate the stiffness degradation more scientifically, two definitions[14] of lateral stiffness, namely equivalent stiffness and peak stiffness, are adopted herein for WH-2. The stiffness degradation curves of the two test walls are shown in Fig. 7.

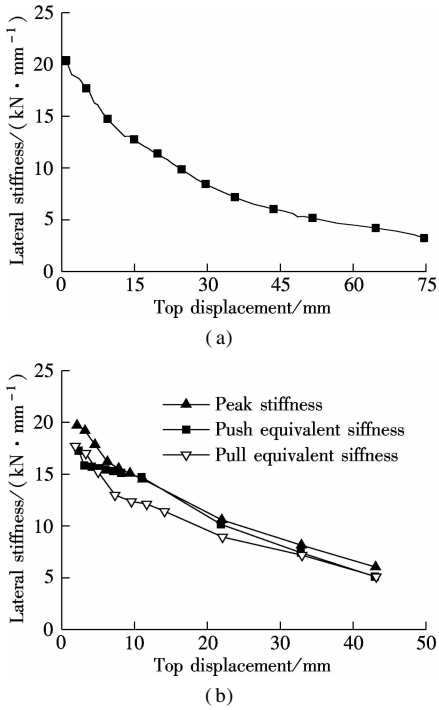

Fig. 7 Degradation of lateral stiffness. (a) WH-1; (b) WH-2

It can be known from Fig. 7 that: 1) The lateral stiffness of WH-1 decayed rapidly at the initial loading stage while reduced gently at the later stage of the loading procedure; and 2) The equivalent stiffness and peak stiffness in both pull and push directions for WH-2 present the same variation tendency with the increase in the top displacement.

3.4 Strain analysis

3.4.1 Strains of the steel bars

The relationships between the strains of the steel bars and the top displacement in WH-1 are shown in Fig. 8. It can be known from Fig. 8 that: 1) The strains of the vertical steel bars increase gradually with the top displacement, and the steel bars successively yield from the outmost (No. 1) to the inside (No. 7) while Nos. 8-11 steel bars are always compressed throughout the loading procedure. Thus, the conclusion can be drawn that the neutral axis is located between the No. 7 and No. 8 steel bars when the test wall fails; and 2) All horizontal steel bars are tensioned and unlikely to yield throughout the whole loading procedure.

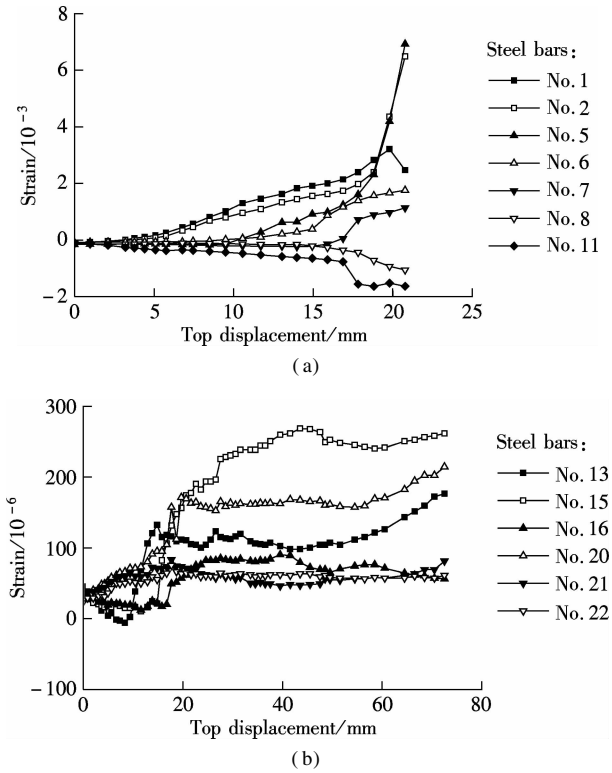

Fig. 8 Relationship between the strains of steel bars and top displacement in WH-1. (a) Vertical steel bars; (b) Horizontal steel bars

3.4.2 Strain distribution in the CSF

Fig. 9 schematically shows the normal and shear strain distributions in the CSF in WH-1. It can be known from the figures that: 1) The CSF is entirely compressed at the

initial loading stage due to the action of the constant vertical load. However, after the test wall yielded, the pressure stress markedly increases in the compressive zone while the tensile stress in the tensile zone is relatively small and remains stable, especially after the top displacement reaches $3\Delta_y$; 2) When the test wall reaches the peak point on its P-Δ curve, the neutral axis of the CSF is within −180 to 180 mm; and 3) The shear stress in the tensile zone is much smaller than that in the compressive zone.

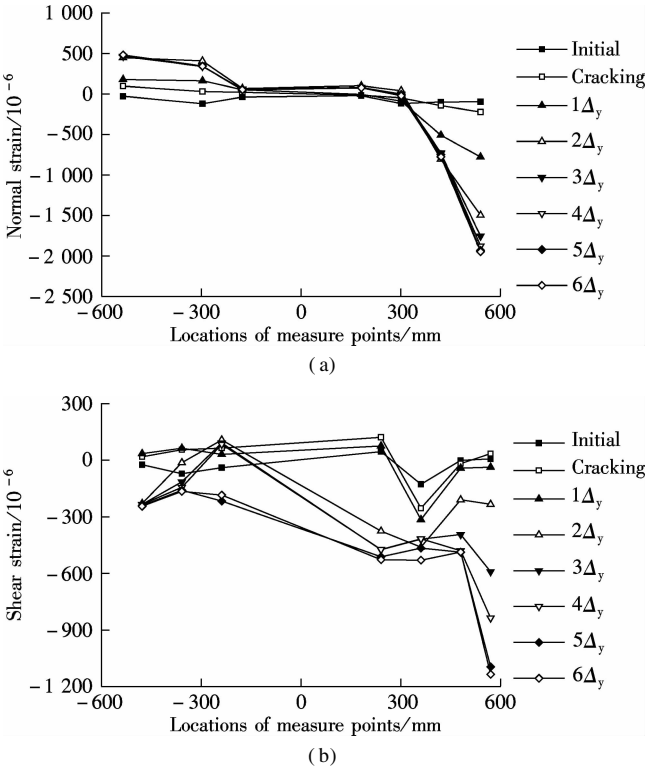

Fig. 9 Strain distribution in the CSF in WH-1. (a) Normal strain; (b) Shear strain

3.5 Slippages between the ELSF and CSF

The relative slippages between the CSF and ELSF in WH-1 are shown in Fig. 10. It can be known from the figure that: 1) The relative slippage between the ELSF and CSF at the UWP bottom on the compression side (measured by DI1) is mainly occurring during the top displacement is 5.09 to 8.49 mm and eventually reaches about 0.5 mm; 2) The relative slippage between the ELSF and CSF at the LWP top on the compression side (measured by DI2) mainly occurring during the top displacement is 2.10 to 27.69 mm and eventually reaches about 1.13 mm; and 3) According to DI3, there is hardly any slippage between the ELSF and CSF at the UWP bottom on the tension side of the test wall.

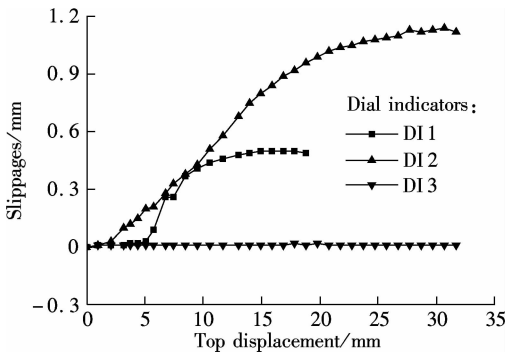

Fig. 10 Relative slippages between the ELSF and CSF

4 Conclusions

1) The novel scheme of the horizontal joints in the IPSW system is both feasible and reliable. The connecting components, including ELSF, HSB, and CSF, can effectively join the adjacent UWP and LWP together.

2) The stress in the connecting components is generally far smaller than the yield stress; and the normal and shear stresses on the compression side of the CSF are much larger than those on its tension side when the test wall moves into the elastic-plastic phase.

3) No relative slippage occurs between the ELSF and CSF on the tension side of the test wall, while the relative slippages on the compression side reaches 0.50 and 1.13 mm at the UWP bottom and LWP top, respectively.

References

[1] Pavese A, Bournas D A. Experimental assessment of the seismic performance of a prefabricated concrete structural wall system [J]. *Engineering Structures*, 2011, **33**(6): 2049 − 2062.

[2] Bora C, Oliva M G, Nakaki S D, et al. Development of a precast concrete shear-wall system requiring special code acceptance [J]. *PCI Journal*, 2007, **52**(1): 122 − 135.

[3] Smith B J, Kurama Y C, McGinnis M J. Design and measured behavior of a hybrid precast concrete wall specimen for seismic regions [J]. *Journal of Structural Engineering*, 2011, **137**(10): 1052 − 1062.

[4] Kurama Y C, Pessiki S, Sause R, et al. Seismic behavior and design of unbonded post-tensioned precast concrete walls [J]. *PCI Journal*, 1999, **44**(3): 72 − 89.

[5] Kurama Y C, Sause R, Pessiki S, et al. Lateral load behavior and seismic design of unbonded post-tensioned precast concrete walls [J]. *ACI Structural Journal*, 1999, **96**(4): 622 − 632.

[6] Kurama Y C, Sause R, Pessiki S, et al. Seismic response evaluation of unbonded post-tensioned precast walls [J]. *ACI Structural Journal*, 2002, **99**(5): 641 − 651.

[7] Perez F J, Sause R, Pessiki S. Analytical and experimental lateral load behavior of unbonded post-tensioned precast concrete walls [J]. *Journal of Structural Engineering*, 2007, **133**(11): 1531 − 1540.

[8] Zhu Z F, Guo Z X. Seismic test and analysis of joints of new precast concrete shear wall structures [J]. *China Civil Engineering Journal*, 2012, **45**(1): 69 − 76. (in Chinese)

[9] Jiang Q, Ye X G, Chong X. Calculation model for superimposed slab shear walls [J]. *China Civil Engineering Journal*, 2012, **45**(1): 8 − 12. (in Chinese)

[10] Sun J, Qiu H X, Xu J P. Experimental and theoretical study on shear capacity of vertical joints in IPSW system [J]. *Journal of Southeast University*: *Natural Science Edition*, 2014, **44**(3): 631－637. (in Chinese)
[11] Ministry of Housing and Urban-Rural Department of the People's Republic of China. GB 50011—2010 Code for seismic design of buildings[S]. Beijing: China Architecture & Building Press, 2010. (in Chinese)
[12] Feng F. Research on seismic performance of precast concrete shear wall structure [D]. Nanjing: School of Civil Engineering of Southeast University, 2012. (in Chinese)
[13] Liu J B, Chen Y G, Guo Z X, et al. Test on seismic performance of precast concrete shear wall with U-shaped closed reinforcements connected in horizontal joints [J]. *Journal of Southeast University*: *Natural Science Edition*, 2013, **43**(3): 565－570. (in Chinese)
[14] Fang Y Z, Gu Q, Shen L. Hysteretic behavior of simi-rigid composite steel frame with reinforced concrete infill wall in column weak axis [J]. *Journal of Building Structures*, 2008, **29**(2): 51－62. (in Chinese)

新型全装配式剪力墙结构水平接缝试验验证

孙　建[1]　邱洪兴[1]　陆　波[2]

([1] 东南大学混凝土及预应力混凝土结构教育部重点实验室, 南京 210096)
([2] 苏州设计研究院股份有限公司, 苏州 215021)

摘要:为了研究新型全装配式剪力墙结构体系中水平接缝的可行性及抗震性能,制作了 2 个试件并分别进行单调加载试验与低周反复加载试验. 在试验的基础上研究了该全装配式剪力墙的荷载-位移曲线、承载能力、延性性能、抗侧刚度、钢筋应变、连接钢框的应变分布以及连接钢框与内嵌边框之间的相对滑移等. 试验结果表明:试件具有较好的承载能力及延性,位移延性系数达 3.7 以上;在整个试验过程中,除受压端外,连接钢框中的正应力及剪应力远小于其屈服强度;试件受压端内嵌边框与连接钢框之间发生了一定的相对滑移,达 1.13 mm,而受拉端二者之间未发生明显的相对滑移. 该全装配式剪力墙结构体系的水平接缝安全可靠,抗震性能良好,方案可行.

关键词:装配式剪力墙;水平接缝;抗震性能;可行性
中图分类号:TU398.2